Journal Name

ARTICLE

Tailoring exciton diffusion and domain size in photovoltaic small molecules by annealing

Received 00th January 20xx,
Accepted 00th January 20xx

DOI:

www.rsc.org/

Muhammad T. Sajjad,[a†] Yiwei Zhang,[a†] Paul B. Geraghty,[b] Valerie D. Mitchell,[b] Arvydas Ruseckas[a], Oskar Blaszczyk[a], David J. Jones*[b] and Ifor D. W. Samuel *[a]

Exciton diffusion is an important part of light harvesting in organic photovoltaics (OPVs) because it enables excitons to reach the interface betweeen donor and acceptor and contribute to the photocurrent. Here we used simple and cost-effective techniques of thermal annealing and solvent vapour annealing to increase the exciton diffusion coefficient and exciton diffusion length in two liquid crystalline electron donor materials BQR and BTR. We found that the three-dimensional exciton diffusion length increased to ~40 nm upon annealing in both materials. Grazing-incidence wide angle X-ray scattering (GIWAXS) measurements show an increase of crystallite size to ~37 nm in both materials after thermal annealing. We determined an average domain size of these materials in the blends with $PC_{71}BM$ using diffusion-limited fluorescence quenching and found that it increased to 31 nm in BTR $PC_{71}BM$ blends and to 60 nm in BQR $PC_{71}BM$ blends. Our results provide understanding of how annealing improves device efficiency.

Introduction,

Organic photovoltaics (OPVs) is a very active field of research because of its potential to give a lightweight, flexible and low-cost source of renewable energy. The development of narrow bandgap electron donor materials and non-fullerene acceptors[1-4] has pushed the power conversion efficiency (PCE) of single junction solar cells to more than 15%,[5] which is good enough for their practical applications. Further improvement of the devices requires optimisation of every step of operation from photon absorption to charge extraction. Annealing is extensively used in the fabrication of OPVs devices. Here we explore its effect on exciton diffusion, crystallinity and domain size to understand how it improves devices.

Exciton diffusion is an important part of light harvesting as it enables excitons to diffuse to the heterojunction of electron donor and acceptor in order to generate electron-hole pairs. These pairs have to dissociate into free carriers and get extracted to the right electrodes. Large donor and acceptor domains are beneficial for dissociation of bound pairs and charge extraction, but can be detrimental to charge pair generation as excitons need to diffuse longer distance to a heterojunction to be harvested. Short exciton diffusion length has been a severe limitation to the optimum morphology of bulk heterojunctions.[6-11]

Approaches to increasing exciton diffusion length include enhancing the lifetime of excited state, suppression non-radiative decay and reducing energetic and positional disorder.[7, 12, 13] Thermal annealing and exposure to solvent vapor have been shown to be simple and effective ways of controlling the exciton diffusion and crystallinity of a film. We have previously used these methods to improve the exciton diffusion and crystallinity of polymer films,[14] and recently to enhance the exciton diffusion length and domain sizes of small molecule OPV blends.[15] However, there are also reports where the exciton diffusion length was reported to decrease upon thermal annealing in small molecules.[16] Every class of materials required different processing methods and optimised conditions. Therefore, a detailed investigation is required to understand the effect of processing on exciton diffusion and domain size in organic semiconductors.

Two electron donor materials benzodithiophene-terthiophene-rhodanine (BTR) and benzodithiophene-quaterthiophene-rhodanine (BQR) have been shown to make efficient solar cells.[17] The molecular structure of BTR and BQR are shown in Figure 1. The efficiency of solar cells have been used as electron donor materials in binary solar cells with 9% efficiency.[17] BTR has also been used as a secondary donor material in ternary blends to make more stable solar cells and to achieve 10.8% efficiency.[18] BTR blends with fullerene showed improvement with solvent vapour annealing which also increased the phase purity and domain size as evident from grazing incidence X-ray diffraction (GIXD) and grazing incidence small angle X-ray scattering (GISAXS) images.[19] However, large domains affect both light harvesting and charge extraction. Therefore it is necessary to understand the effect of annealing on light harvesting especially on exciton diffusion.

Here we investigated the effect of thermal and solvent vapour annealing on the exciton diffusion and on the crystallinity of these small molecules BQR and BTR films. In both molecules, we find that the exciton diffusion coefficient (D) increases upon annealing. The highest increase in D (~ 4 times i.e. from $1.1 \times 10^{-3} cm^2/s$ to $4.0 \times 10^{-3} cm^2/s$) is observed for BTR when the film is annealed using the solvent tetrahydrofuran, which then led to almost doubling

[a] Organic Semiconductor Centre, SUPA, School of Physics & Astronomy, North Haugh, St Andrews, KY16 9SS, United Kingdom
[b] School of Chemistry, Bio21 Institute, University of Melbourne, Parkville, Victoria, Australia, 3010.

Electronic Supplementary Information (ESI) available: Exciton-exciton annihilation data such as intensity dependent time-resolved PL decays of neat donor films before and after annealing and GIWAXS analysis to determine the crystallite size and crystallite coherence length. See DOI: 10.1039/x0xx00000x

† These authors contributed equally

of L_D from ~23 nm to ~40 nm. We measured crystallite size using GIWAXS and found an increase in the crystallite size after annealing.

We also used time-resolved fluorescence measurements to investigate the effect of annealing on domain size of the donor molecules in the blends with $PC_{71}BM$ and found that in BTR it increases by more than a factor of 3 from 7 nm to 25 nm, whereas BQR domains increase in size by a factor of 4 from ~15 nm to 60 nm after SVA. This is normally too large for efficient charge separation. However, the large L_D (>40 nm) means that efficient exciton harvesting still occur.

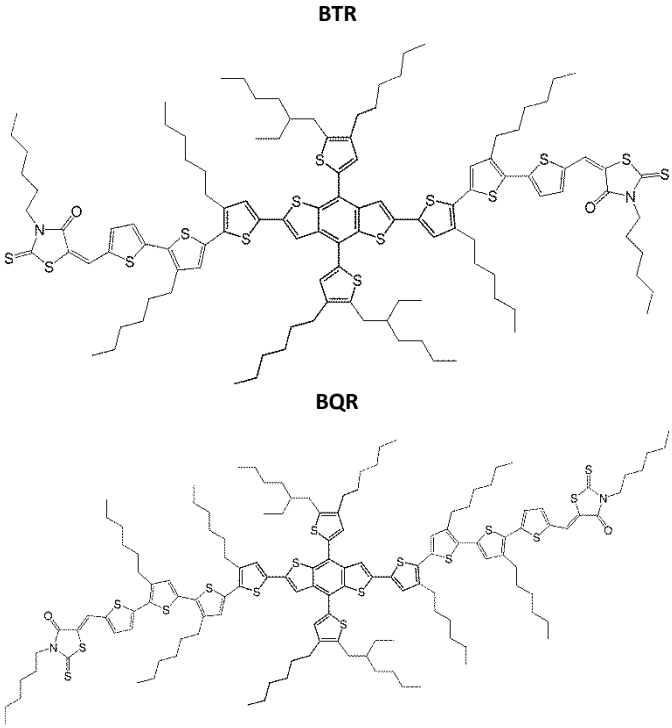

Figure 1: *Molecular structure of BTR and BQR.*

Results and discussion

The absorption spectra of as-cast films of similar thickness are shown in **Figure 2a.** Absorption spectra show that BQR films have a dominant peak around 644 nm (A_{0-0}) and a shoulder around 594 nm (A_{0-1}), whereas BTR has two peaks around 620 nm (A_{0-0}) and around 576 nm (A_{0-1}). Absorption spectra of BQR are red-shifted compared to BTR and this has been assigned to increased conjugation length and more ordering compared to BTR.[17]

To investigate the effect of annealing on the absorption, we have measured absorption spectra of thermal and solvent vapour annealed films. For thermal annealing, a temperature of 120 ^{0}C was used for 10 min and for solvent vapour annealing, two solvents; tetrahydrofuran (THF) and chloroform ($CHCl_3$) were used. After optimisation of conditions for annealing, we measured the absorption of all the films of BQR and the resulting normalised absorption spectra are shown in Figure 2b.

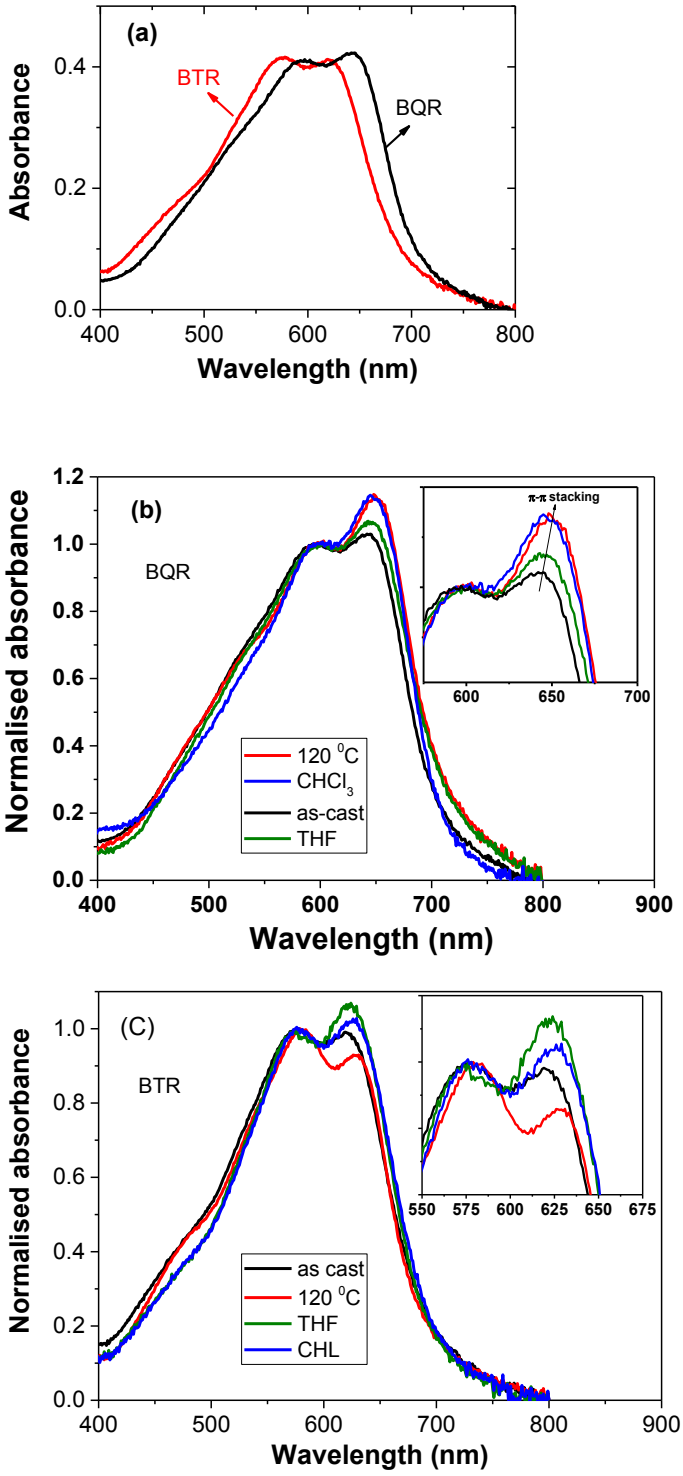

Figure 2: *The absorption spectra of thin films of BTR and BQR. (a) as- cast films of BTR (65.4 nm) and BQR (64.7 nm). (b) BQR films before and after annealing. (c) Absorption spectra of BTR films before and after annealing. Inset is an enhanced area to show increased π-π stacking. Thermally annealed film: 120 ^{0}C for 10 min and SVA with THF and $CHCl_3$ for 10 s.*

After thermal or solvent vapour annealing, the dominant peak around 644 nm increases (an expansion of area around that peak is given in inset). This suggests an increase in conjugation length due to better π-π stacking of the chains after annealing which develops the crystalline order further.[14, 17] The results for BTR are shown in Figure

2c. The peak at 620 nm is increased by solvent vapour annealing but not by thermal annealing. In both molecules, a red-shift of more than 10 nm is observed in the absorption spectra after thermal annealing compared to as-cast film.

We measured the exciton diffusion using exciton-exciton annihilation. In this method time-resolved PL decays are measured at different initial excitation densities. The resulting PL decays are shown in **Figure S1 and S2**. At high initial excitation density, the PL decays are faster because a large number of excitons are created which are close to each other, therefore annihilate faster. The density of singlet excitons created is proportional to time-resolved PL intensity and can be described by the rate equation.

$$\frac{dN}{dt} = G - k(t)N - \gamma(t)N^2 \qquad (1)$$

Here *G* corresponds to exciton generation which is instantaneous in this case (i.e. generation is within the 200 fs duration of the excitation pulse), *k(t)* is the natural decay rate constant in the absence of annihilation and $\gamma(t)$ is the annihilation rate constant. At low excitation density (<10^{15} cm^{-3}) the annihilation term is negligible and so fitting the low excitation density data gives us k(t). As the decay is non-exponential, we used a sum of three exponentials to obtain k(t). We then fit all the decays at high excitation densities (>10^{16} cm^{-3}) to obtain $\gamma(t)$. The annihilation rate constants $\gamma(t)$ obtained for both molecules before and after annealing are shown in Figure 3a and 3b. In both molecules, $\gamma(t)$ is strongly time-dependent at early times and becomes time-independent at longer time (> 200ps). This is similar to the behaviour observed previously in organic semiconductors, where early time annihilation is controlled by direct transfer and longer time annihilation is controlled by exciton diffusion. [14, 15, 20, 21] The comparison of $\gamma(t)$ at longer time (> 200ps) indicates that films annealed (either thermally or by solvent vapour) have higher exciton diffusion compared to as-cast film in both molecules. The highest $\gamma(t)$ for BTR is for SVA with THF. For BQR the highest $\gamma(t)$ is for $CHCl_3$.

The value of exciton diffusion coefficient (D) was extracted by describing the diffusion-limited annihilation in a three-dimensional isotropic system by the sum of time-dependent and time-independent terms,

$$\gamma(t) = 4\pi R_a D\left(1 + \frac{R_a}{\sqrt{2\pi Dt}}\right) \qquad (2)$$

where *D* is the exciton diffusion coefficient and R_a is the annihilation radius. For Ra, we used the d_{100}-spacing values obtained from GIWAXS data. These values are given in Table S1. The resulting values of diffusion coefficients are shown in Figure 4.

For the case of BQR, a diffusion coefficient of $3.0 \times 10^{-3} cm^2/s$ was obtained for the as-cast donor film (without annealing). After thermal annealing the diffusion coefficient increased to $3.8 \times 10^{-3} cm^2/s$, and after SVA it was $3.3 \times 10^{-3} cm^2/s$ for THFand $5.0 \times 10^{-3} cm^2/s$ for $CHCl_3$. In the case of BTR, the as-cast donor film has a diffusion coefficient of $1.1 \times 10^{-3} cm^2/s$. The diffusion coefficient after thermal annealing was $1.5 \times 10^{-3} cm^2/s$ and after SVA was $4.0 \times 10^{-3} cm^2/s$ for THF and $3.5 \times 10^{-3} cm^2/s$ for $CHCl_3$. Overall, D increases after annealing (both thermal and SVA) in both molecules. In the case of BQR, the largest increase is observed for $CHCl_3$ which leads to an almost doubling of D, whereas a tripling of D for BTR was observed when annealed with SVA THF.

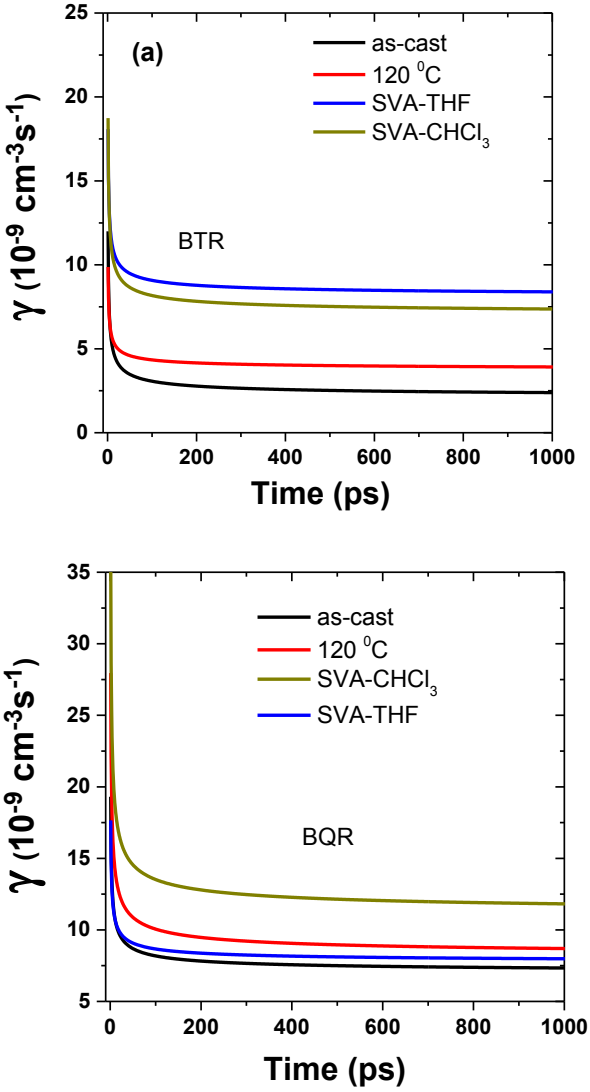

Figure 3: *Annihilation rate constant γ, obtained from the fitting of the intensity-dependent PL decays (shown in figure S1 and S2) using equation 1. (a) BTR b) BQR*

We calculated the exciton diffusion length (L_D). In bulk heterojunction geometry, the three-dimensional exciton diffusion is relevant, therefore we determine the three-dimensional exciton diffusion length (L_{3D}) using $L_{3D} = \sqrt{6D\tau}$, where τ is the lifetime in the absence of annihilation. The PL decays are non-exponential, so we take τ to be the time when the PL decays to 1/e of its initial value. The results are summarised in table 1. In the case of BQR, all the films showed an L_{3D} between 39 nm and 43 nm, whereas, in the case of BTR, an L_{3D} of 24 nm was obtained for the as-cast film (without annealing) and for thermally annealed film. However this L_{3D} increases to 33 nm for SVA with $CHCl_3$ film and to 42 nm for SVA with THF. The higher value in both molecules after SVA may be due to the higher crystallinity of the films after SVA. In both molecules, an L_{3D} of more than 40 nm was obtained after SVA which is comparable to the previously reported value for the small molecule DR3TBDTT.[15] This shows that with the assistance of SVA substantial exciton diffusion lengths can be achieved in a range of small molecule OPV materials.

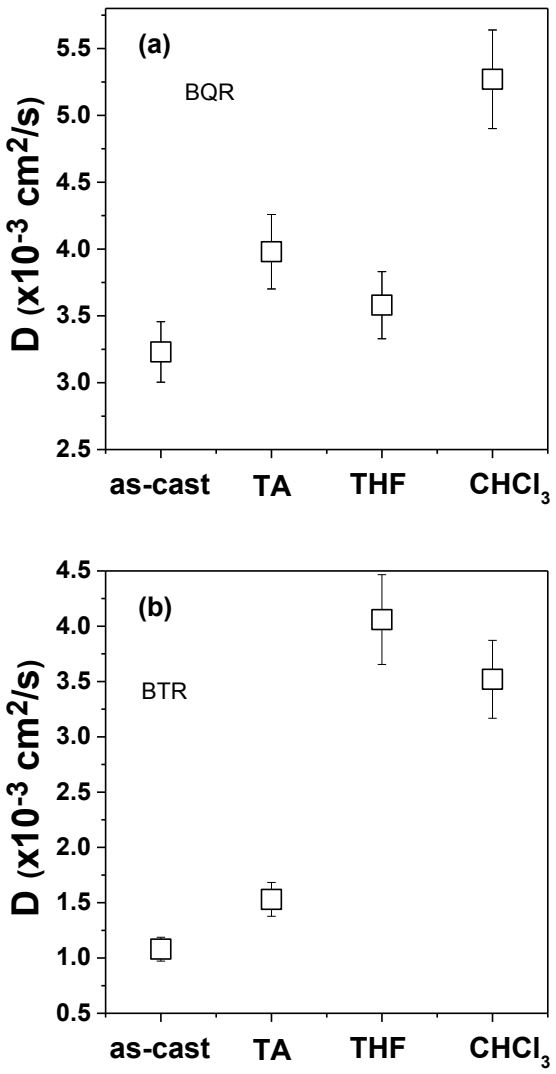

Figure 4: *Exciton diffusion coefficient (D) in all films of both molecules, determined using eq.2.TA is for a thermally annealed film.*

We investigated possible changes in the film by Grazing incidence Wide Angle X-ray scattering (GIWAXS). The 2D GIWAXS image of the as-cast BTR film is shown in Figure 5. It has two distinct features; the reflections around ~ 3 nm^{-1} and ~ 7 nm^{-1} are attributed to the lamellar (100) and (200) crystalline planes.[23, 24] They are stronger in the out of plane direction i.e. in the q_z direction, which indicates the edge on orientation of chains onto the substrate. The Bragg peak around 17 nm^{-1} (010) is attributed to π-π stacking and is stronger in the in- plane i.e. in the q_{xy} direction. After the thermal and solvent vapour annealing, the peaks narrow (Figure S3) and increase in intensity which indicates better crystallinity (Figure 5). There are also additional reflections in the annealed films which further suggest better organized crystallites.

The crystallite size was calculated using Williamson-Hall analysis by considering FWHM of (h00) q_z reflections as a function of the reflection order squared (detail given in the experimental section). The results are given in table 1. Thermally annealed film leads to an enhancement of 54% in the crystallite size compared to as-cast film, whereas, solvent vapour annealing leads to 8% enhancement in the crystallite size.

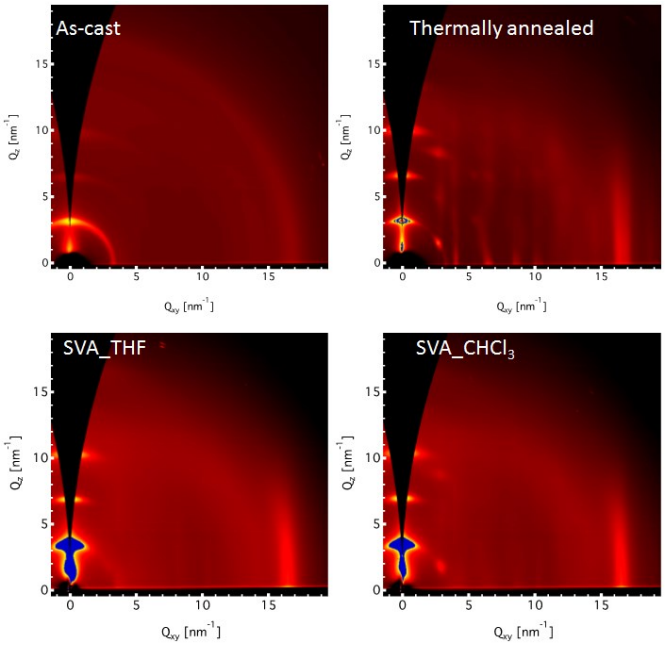

Figure 5: *Grazing incidence Wide Angle X-ray scattering images (GIWAXS) images of thin films of BTR before and after thermal and solvent vapour annealing. SVA_THF is for solvent vapour annealing using tetrahydrofuran and SVA _$CHCl_3$ for solvent vapour annealing with chloroform solvent.*

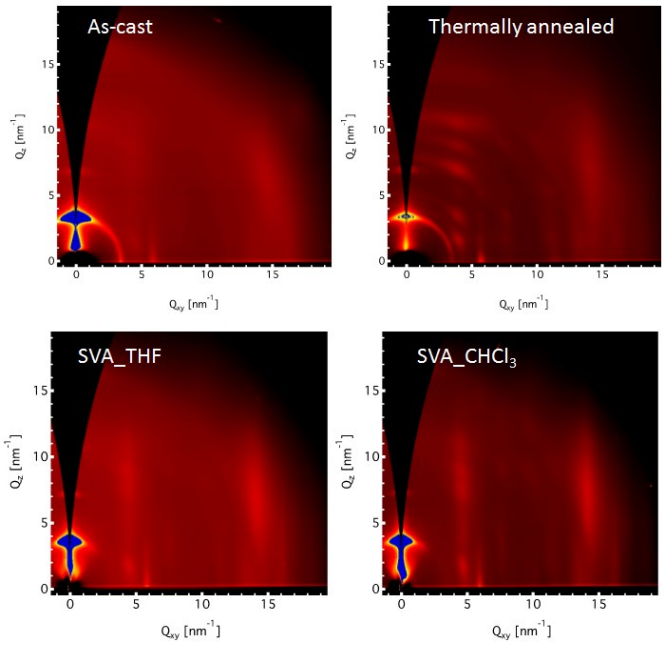

Figure 6: *Grazing incidence Wide Angle X-ray scattering images (GIWAXS) images of thin films of BQR before and after thermal and solvent vapour annealing. SVA_THF is for solvent vapour annealing using tetrahydrofuran and SVA _$CHCl_3$ for solvent vapour annealing with chloroform solvent.*

We have also performed GIWAXS on BQR samples and 2D GIWAXS images are shown in Figure 6. The noticeable features are enhanced (100) reflections in the q_z axis of the SVA films. This is an indication of slightly more edge on orientation compared to as-cast film. The calculated value of crystallite size are summarized in Table 1. Thermal annealing led to more than a doubling of crystallite size to 37.4 nm, whereas, SVA increased crystallite size to 25 nm (~39%).

Table 1 shows that for several experiments the crystallite size increases on annealing. The diffusion coefficient increases in all experiments but there is little correlation between them. This could be because crystallite size is not an adequate description of ordering of the film relevant to exciton diffusion.

Table 1: Exciton diffusion coefficient (D), 1/e lifetime (τ), three-dimensional diffusion length (L_{3D}), and *crystallite size (L_c) in neat films.*

Sample name	D (x10^{-3} cm^2/s)	τ (ps)	L_{3D} (nm)	L_c (nm)
BQR_as-cast	3.0	840	39	18
BQR_TA	3.8	765	42	37
BQR_SVA-THF	3.4	777	40	25
BQR_SVA-$CHCl_3$	5.0	583	43	25
BTR_as-cast	1.1	810	23	24
BTR_TA	1.6	750	27	37
BTR_SVA-THF	4.0	680	40	26
BTR_SVA-$CHCl_3$	3.5	450	31	25

In summary annealing increases D. This can enhance exciton harvesting and hence device performance. Previous studies reported that solar cells fabricated using these materials showed a significant enhancement in short circuit current (J_{sc}) after thermal and solvent vapour annealing.[17] This enhancement in J_{sc} after annealing suggests better exciton harvesting due to large exciton diffusion length. However device performance depends on both exciton harvesting and charge extraction. The latter depends on domain size and so we next make an estimate domain size by performing time-resolved PL spectroscopy on the blends. The PL decays of as-cast and annealed (thermally and SVA) blends of both molecules are shown in Figure 5. For comparison, we have also plotted the PL decays of the annealed and as-cast neat donor films. The PL decays of the blends are faster compared to neat donor films due to dissociation of excitons at the interface between donor and acceptor. In both molecules, the as-cast blends show faster decay suggesting smaller domains whereas, the blends annealed using either $CHCl_3$ (BQR) or THF solvents show slower decay indicating larger domains.

The domain size of donor molecules was extracted using an approach similar to Hedley et al[6] and Jagadamma et al[25] by considering that PL quenching of the donor in the blend is exciton diffusion limited. We assumed that the sphere of the donor is surrounded by a $PC_{71}BM$ matrix. The exciton diffuses by a random walk inside the sphere and is quenched at the interface with $PC_{71}BM$. Then the decay of the number of excitons *N(t)* on donor molecules with time follows as

$$N(t) = \frac{6}{\pi^2}\sum_{m=1}^{\infty}\frac{1}{m^2}\,exp\left(\frac{-D\pi^2 m^2 t}{r^2}\right) \qquad (3)$$

where *D* is the exciton diffusion coefficient and *r* is the radius of the sphere. We used the experimentally measured values of D for as-cast and annealed films.

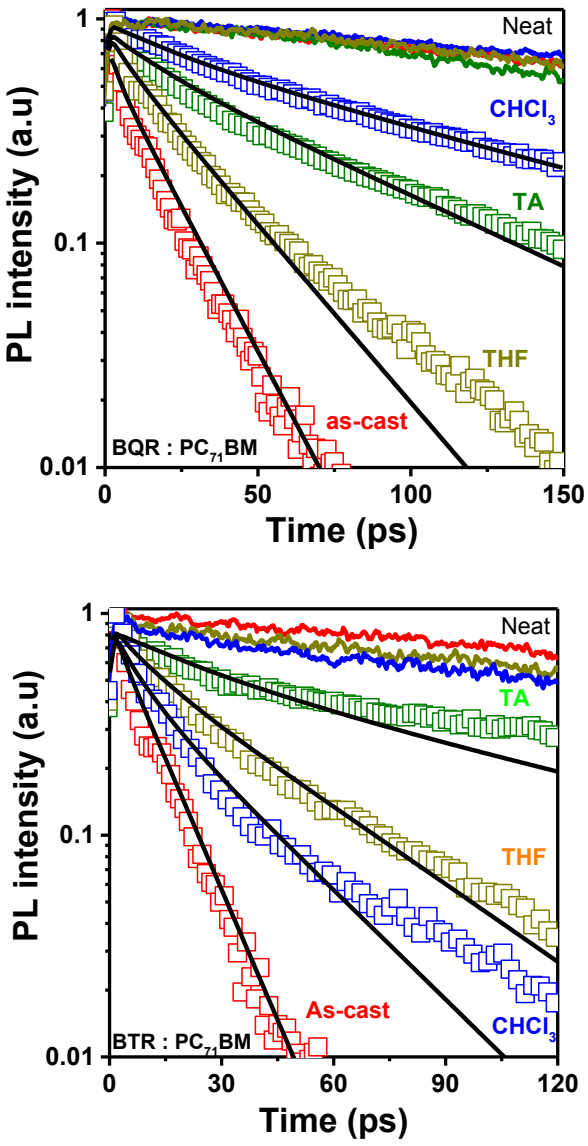

Figure 5: *Time-resolved PL quenching of as-cast blends and after thermal and SVA (colour dots). The PL decays of neat donors before and after annealing are also plotted (colour solid lines). Average domain size of donors was extracted by fitting the PL quenching data using eq.3 (solid black lines). (a) BQR and (b) BTR*

Equation 3 was multiplied by the fluorescence intensity of the neat donors and then used to fit the PL decays of the blends. For the case of BQR: $PC_{71}BM$, the domain size of donor molecules increased from ~15 nm to ~60 nm after annealing with $CHCl_3$ SVA. Whereas, in the case of BQR: $PC_{71}BM$, donor domains increased from ~7 nm to ~26 nm after annealing with THF solvent.

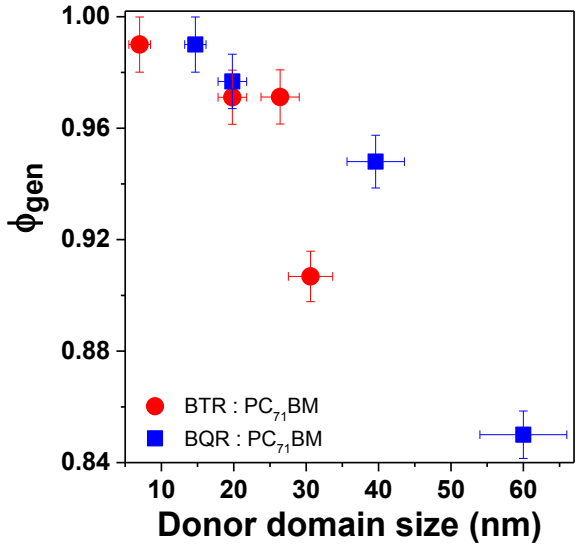

Figure 7: Estimated *charge generation efficiency as a function of average donor domain size in the blends*

The large domains normally reduce the charge generation efficiency which then leads to lower device efficiency. We estimated the charge generation efficiency from the PL decays of the neat donors and their blends with $PC_{71}BM$ using

$$\emptyset_{gen} = 1 - \frac{\tau_{blend}}{\tau_{neat}}$$

where τ_{blend} is the lifetime of blend and τ_{neat} is the lifetime of neat donor film. As the decay is multiexponential, therefore we used 1/e lifetimes. In this estimate we assume all excitons quenched generate charges. The estimated charge generation efficiency is plotted as a function of domain size in Figure 6, which shows efficient charge generation (84%) despite the large domains (60 nm). This is due to large exciton diffusion length (> 40 nm) which enables most of the generated excitons to reach the interface in their lifetime and split into free charges. Large domain sizes lead to the reduced interface area between donor and acceptor and can explain strongly suppressed bimolecular recombination observed in BTR:$PC_{71}BM$ solar cells.[26] Development of processing techniques which increase exciton diffusion length and domain sizes is a viable approach to develop more efficient organic solar cells.

Experimental

Materials

BTR, BQR was synthesized using the methods reported before.[17, 22] All the solvent was purchased from Sigma Aldrich.

Sample preparation

For untreated and thermally annealed samples, the materials were dissolved in chloroform at a concentration of 10 mg/ml.For solvent vapour annealed samples, materials were dissolved in chloroform at a concentration of 4mg/ml in chloroform. The solution was stirred at room temperature overnight to ensure full dissolving before spin coating on to pre-cleaned fused silica substrates in a nitrogen-filled glovebox. The films were made by spin coating the solution at 1500 rpm for 40s. The thermal annealing was conducted using a hot plate setting at 120 °C for 10 minutes. Solvent vapour annealing was performed using the following procedure: first drop ~200 µl tetrahydrofuran /chloroform into a petri-dish; then put the samples onto a platform surrounded by the solvent; finally, close the lid and keep the samples inside the solvent atmosphere for 30 seconds.

Absorption, Exciton diffusion and PL quenching measurements

Absorption spectra were measured using a Cary 300 UV-visible spectrophotometer. Time-resolved fluorescence was recorded using a Hamamatsu C10190 streak camera. For exciton diffusion measurements, the films were excited by 200 fs laser pulses at 630 nm with 50 kHz repetition rate. The pulses were generated using an optical parametric amplifier pumped by a Pharos regenerative amplifier from Light Conversion Ltd. For PL quenching measurements in the blends the samples were excited by 200 fs laser pulses at 645 nm to avoid excitation of $PC_{71}BM$.

Grazing Incidence Wide Angle X-ray Spectroscopy

GIWAXS measurements were conducted at the SAXS/WAXS beamline of the Australian synchrotron. The substrates were silicon wafers that had been sonicated in acetone and isopropanol for 10 min each followed by 3 min oxygen plasma for as-cast and thermally annealed films. For solvent vapour annealing, substrates were sonicated in acetone and isopropanol for 30 min each followed by 15 min of UV/ozone treatment. The measurements were performed with an X-ray energy of 11 keV and a range of incident angles from Ω = 0.025–0.5 in 0.01-0.05 increments to allow signal optimization near the critical angle of the polymer film but below the critical angle of the substrate. Data from GIWAXS experiments were analyzed using a customized version of NIKA 2D[27] based in IgorPro.

Crystallite size calculation

To calculate the average crystallite size, we fit each (h00) peak (e.g., **Figure S2c**) to a Gaussian function. We then fit the full width half max (fwhm) of each peak as a function of *h*(order of diffraction) squared using a linear fit. The slope of such a fit is related to the non-uniform strain of the crystallite, while the intercept is inversely proportional to the average crystallite size according to:

L_C =2 PiK/b

Here L_C is the crystallite size, *K* is a constant and assumed here to be ~ 1, and *b* is the intercept extracted from the linear fit described above.

Conclusions

We have shown that processing can enhance exciton diffusion, crystallinity and domain size. We observed more than 4 times enhancement in exciton diffusion coefficient and almost doubling of exciton diffusion length after annealing to obtain 3D exciton diffusion lengths of up to 43 nm. We also found that annealing increases the domain size of the donor in the blend. Because the increase in domain size is accompanied by an increase in exciton diffusion, charge generation remains efficient (> 80%) even for large domains (60 nm).

Conflicts of interest

There are no conflicts to declare.

Acknowledgements

We acknowledge support from the European Research Council (grant 321305). We are grateful to EPSRC for equipment grant (EP/L017008/1) and for support of OB (EP/M508214/1).

This work was made possible by support from the Australian Renewable Energy Agency which funds the project grants within the Australian Centre for Advanced Photovoltaics. Responsibility for the views, information or advice expressed herein is not accepted by the Australian Government. We acknowledge the SAXS/WAXS beamline at the Australian Synchrotron.

The research data supporting this publication can be accessed at 10.17630/10fd3801-b282-42c9-b672-750f8d1bb635

Notes and references

1. S. Li, L. Ye, W. Zhao, S. Zhang, S. Mukherjee, H. Ade and J. Hou, *Advanced Materials*, 2016, **28**, 9423-9429.
2. Y. Lin, J. Wang, Z. G. Zhang, H. Bai, Y. Li, D. Zhu and X. Zhan, *Advanced materials*, 2015, **27**, 1170-1174.
3. H. Yao, Y. Cui, R. Yu, B. Gao, H. Zhang and J. Hou, *Angewandte Chemie International Edition*, 2017, **56**, 3045-3049.
4. S. Dai, F. Zhao, Q. Zhang, T.-K. Lau, T. Li, K. Liu, Q. Ling, C. Wang, X. Lu and W. You, *J. Am. Chem. Soc.*, 2017, **139**, 1336-1343.
5. J. Yuan, Y. Zhang, L. Zhou, G. Zhang, H.-L. Yip, T.-K. Lau, X. Lu, C. Zhu, H. Peng, P. A. Johnson, M. Leclerc, Y. Cao, J. Ulanski, Y. Li and Y. Zou, *Joule*, (in press).
6. G. J. Hedley, A. J. Ward, A. Alekseev, C. T. Howells, E. R. Martins, L. A. Serrano, G. Cooke, A. Ruseckas and I. D. Samuel, *Nat. Commun.,* 2013, ***4, 2867***.
7. G. J. Hedley, A. Ruseckas and I. D. Samuel, *Chem. Rev.,* 2017, ***117***, 796-837
8. B. Walker, A. B. Tamayo, X. D. Dang, P. Zalar, J. H. Seo, A. Garcia, M. Tantiwiwat and T. Q. Nguyen, *Adv. Funct. Mater.*, 2009, **19**, 3063-3069.
9. J. T. Rogers, K. Schmidt, M. F. Toney, E. J. Kramer and G. C. Bazan, *Adv. Mater.*, 2011, **23**, 2284-2288.
10. Y. Sun, C. Cui, H. Wang and Y. Li, *Adv. Energy Mater.*, 2011, **1**, 1058-1061.
11. M. Li, F. Liu, X. Wan, W. Ni, B. Kan, H. Feng, Q. Zhang, X. Yang, Y. Wang and Y. Zhang, *Adv. Mater.*, 2015, **27**, 6296-6302.
12. Y. Tamai, H. Ohkita, H. Benten and S. Ito, *J. Phys. Chem. Lett.,* 2015, **6**, 3417-3428
13. O. V. Mikhnenko, P. W. Blom and T.-Q. Nguyen, *Energy Environ. Sci.,* 2015, **8**, 1867-1888.
14. M. Chowdhury, M. T. Sajjad, V. Savikhin, N. Hergue, K. Sutija, S. Oosterhout, M. F. Toney, A. Ruseckas and I. D. Samuel, *Phys. Chem. Chem. Phys.,* 2017, **19**, 12441-12451.
15. M. T. Sajjad, O. Blaszczyk, L. K. Jagadamma, T. J. Roland, M. Chowdhury, A. Ruseckas and I. D. Samuel, *J. Mater. Chem. A*, 2018, **6**, 9445-9450.
16. O. V. Mikhnenko, J. Lin, Y. Shu, J. E. Anthony, P. W. Blom, T.-Q. Nguyen and M. A. Loi, *Phys. Chem. Chem. Phys.*, 2012, **14**, 14196-14201.
17. P. B. Geraghty, C. Lee, J. Subbiah, W. W. Wong, J. L. Banal, M. A. Jameel, T. A. Smith and D. J. Jones, *Beilstein journal of organic chemistry*, 2016, **12**, 2298.
18. X. Ma, F. Zhang, Q. An, Q. Sun, M. Zhang, J. Miao, Z. Hu and J. Zhang, *J. Mater. Chem. A*, 2017, **5**, 13145-13153.
19. S. Engmann, H. W. Ro, A. Herzing, C. R. Snyder, L. J. Richter, P. B. Geraghty and D. J. Jones, *J. Mater. Chem. A*, 2016, **4**, 15511-15521.
20. P. E. Shaw, A. Ruseckas and I. D. Samuel, *Adv. Mater.*, 2008, **20**, 3516-3520.
21. Z. Masri, A. Ruseckas, E. V. Emelianova, L. Wang, A. K. Bansal, A. Matheson, H. T. Lemke, M. M. Nielsen, H. Nguyen and O. Coulembier, *Adv. Energy Mater.*, 2013, **3**, 1445-1453.
22. K. Sun, Z. Xiao, S. Lu, W. Zajaczkowski, W. Pisula, E. Hanssen, J. M. White, R. M. Williamson, J. Subbiah and J. Ouyang, *Nat. Commun.*, 2015, **6**, 6013.
23. J. Rivnay, S. C. Mannsfeld, C. E. Miller, A. Salleo and M. F. Toney, *Chem. Rev.*, 2012, **112**, 5488-5519.
24. D. T. Duong, V. Ho, Z. Shang, S. Mollinger, S. C. Mannsfeld, J. Dacuña, M. F. Toney, R. Segalman and A. Salleo, *Adv. Funct. Mater.*, 2014, **24**, 4515-4521.
25. L. K. Jagadamma, M. T. Sajjad, V. Savikhin, M. F. Toney and I. D. Samuel, *J. Mater. Chem. A*, 2017, **5**, 14646-14657.
26. A. Armin, J. Subbiah, M. Stolterfoht, S. Shoaee, Z. Xiao, S. Lu, D. J. Jones and P. Meredith, *Adv.Energy Mater.*, 2016, **6**, 1600939.
27. J. Ilavsky, *J. Appl. Crystallography*, 2012, **45**, 324-328.